J. Fluid Mech. (2011), *vol.* 680, *pp.* 459–476.
doi:10.1017/jfm.2011.172

Influence of slip on the flow past superhydrophobic circular cylinders

PRANESH MURALIDHAR, NANGELIE FERRER, ROBERT DANIELLO AND JONATHAN P. ROTHSTEIN†

Department of Mechanical and Industrial Engineering, University of Massachusetts Amherst, Amherst, MA 01003, USA

(Received 6 October 2010; revised 15 February 2011; accepted 6 April 2011; first published online 24 May 2011)

Superhydrophobic surfaces have been shown to produce significant drag reduction for both laminar and turbulent flows of water through large- and small-scale channels. In this paper, a series of experiments were performed which investigated the effect of superhydrophobic-induced slip on the flow past a circular cylinder. In these experiments, circular cylinders were coated with a series of superhydrophobic surfaces fabricated from polydimethylsiloxane with well-defined micron-sized patterns of surface roughness. The presence of the superhydrophobic surface was found to have a significant effect on the vortex shedding dynamics in the wake of the circular cylinder. When compared to a smooth, no-slip cylinder, cylinders coated with superhydrophobic surfaces were found to delay the onset of vortex shedding and increase the length of the recirculation region in the wake of the cylinder. For superhydrophobic surfaces with ridges aligned in the flow direction, the separation point was found to move further upstream towards the front stagnation point of the cylinder and the vortex shedding frequency was found to increase. For superhydrophobic surfaces with ridges running normal to the flow direction, the separation point and shedding frequency trends were reversed. Thus, in this paper we demonstrate that vortex shedding dynamics is very sensitive to changes of feature spacing, size and orientation along superhydrophobic surfaces.

Key words: drag reduction, separated flows, vortex shedding

1. Introduction

The flow past a circular cylinder is a benchmark problem in fluid dynamics which has been studied for well over a hundred years with seminal works coming from Strouhal (1878), Bénard (1908) and von Kármán (1911) amongst others (Williamson 1996). As a representative bluff body, studies of flow over a circular cylinder have proved to be instrumental in gaining a fundamental understanding of a broad class of flows where flow separation and vortex shedding occur. At high Reynolds numbers, the onset of vortex shedding is accompanied by a number of unwanted and potentially damaging consequences including increased drag, root mean square (r.m.s.) lift and structural vibrations. As a result, there have been a number of studies which have focused on developing both active and passive strategies for reducing the intensity of these vortex-induced vibrations. In this study, we will use superhydrophobic surfaces

† Email address for correspondence: rothstein@ecs.umass.edu

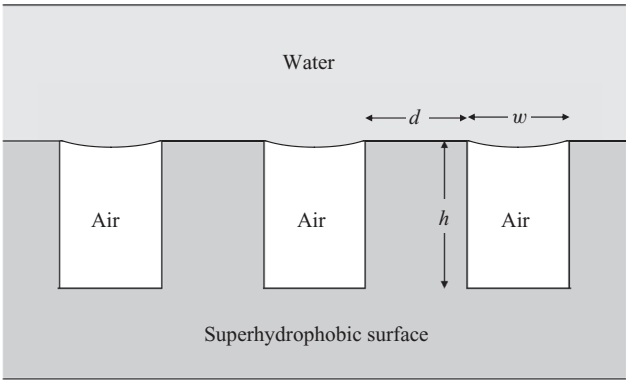

FIGURE 1. Schematic diagram of a superhydrophobic surface in the Cassie state.

to investigate the role that slip and the associated reduction in skin-friction drag plays on the flow past circular cylinders.

Superhydrophobic surfaces were originally inspired by the unique water-repellent properties of the lotus leaf (Barthlott & Neinhuis 1997) and the leaves of a number of other plants (Bhushan & Jung 2006). It is the combination of a very large contact angle and a low contact angle hysteresis that defines a surface as superhydrophobic. The difference between a hydrophobic surface and a superhydrophobic surface lies not in the surface chemistry, but in its micro- or nanoscale surface roughness. Lotus leaves, for example, have micron-sized protrusions covered in waxy crystals while man-made superhydrophobic surfaces are often fabricated using lithographic techniques with precise patterns of micron- or nanometre-sized ridges or posts (Bico, Marzolin & Quere 1999; Oner & McCarthy 2000; Zhang *et al.* 2008; Rothstein 2010). In the Wenzel state (Wenzel 1936), water penetrates into the corrugations on the surface. In the Cassie state (Cassie & Baxter 1944), the hydrophobicity of the small-scale surface roughness prevents the water from moving into the space between the peaks on the surface, resulting in an air–water interface supported between the peaks in the surface roughness. This can be seen schematically in figure 1 and physically in figure 2(*b*), where the interface is visible through a water drop. It is only in the Cassie state that a surface is truly superhydrophobic and it is in the Cassie state that these surfaces have recently been shown to produce significant drag reduction in both laminar and turbulent flows (Rothstein 2010).

In flows over superhydrophobic surfaces, the boundary condition experienced by the fluid in contact with the solid is no-slip; however, the air–water interfaces supported between the surface features are essentially shear-free. Ou, Perot & Rothstein (2004) and Ou & Rothstein (2005) were among the first to experimentally demonstrate that superhydrophobic surfaces could reduce drag in laminar channel flows. Using a series of surfaces with precisely controlled surface topology consisting of regular arrays of micron-sized posts and ridges, they observed drag reductions up to 40 %, slip velocities along the superhydrophobic surface of as much as 60 % of the free-stream velocity and slip lengths up to $b = 25\,\mu\text{m}$. Here the slip length is defined using Navier's slip model (Navier 1823), where the slip velocity, u_0, is proportional to the shear rate experienced by the fluid at the wall, $u_0 = b(\partial u/\partial y)_{y=0}$. Drag reduction and slip length have been found to increase with increasing percentage of shear-free air–water interface, increasing spacing between microfeatures and decreasing channel

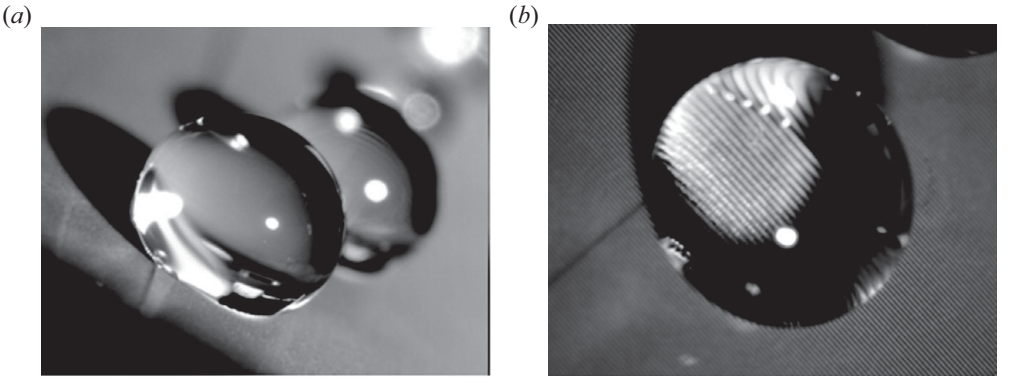

FIGURE 2. Water drops on a superhydrophobic surface consisting of 30 μm wide ridges spaced 30 μm apart seen from the side (*a*) and the top (*b*). Note that the ridges and the air–water interface supported between them are visible through the drop in the top view (*b*).

height (Lauga & Stone 2003; Ou *et al.* 2004; Ou & Rothstein 2005; Choi & Kim 2006; Choi *et al.* 2006; Joseph *et al.* 2006; Truesdell *et al.* 2006; Ybert *et al.* 2007; Rothstein 2010) with slip lengths as large as $b = 400\,\mu$m possible for superhydrophobic surfaces with 98 % air–water interface (Lee & Kim 2009).

Superhydrophobic surfaces have also been shown to reduce drag in turbulent channel flows. In turbulent flows, a thin laminar sublayer exists very near to the wall (Pope 2003). A theoretical analysis by Fukagata, Kasagi & Koumoutsakos (2006) demonstrated how a small alteration of the laminar sublayer can affect the entire turbulent boundary layer and subsequently alter the drag. This effect is demonstrated in the direct numerical simulation (DNS) studies of Min & Kim (Min & Kim 2004), who performed turbulent channel flow simulations with an arbitrary, but not unreasonable, slip length boundary imposed both parallel and perpendicular to the flow direction. Their simulations demonstrated a decrease in wall shear stress with increasing slip length applied parallel to the flow direction, but an increase in wall shear stress for slip applied perpendicular to the flow direction. More recently, Martell, Perot & Rothstein (2009), Martell, Rothstein & Perot (2010) used DNS to study the turbulent channel flows over superhydrophobic surfaces containing periodic arrays of micropost and microridge geometries. As in the laminar case, these simulations showed a slip velocity and drag reduction that increase with both the increasing microfeature spacing and surface coverage of the shear-free air–water interface. However, unlike in laminar flows, in turbulent channel flows, increasing the flow rate and Reynolds number results in an increase in the superhydrophobic drag reduction (Martell *et al.* 2010).

There are also a few experimental studies of superhydrophobic drag reduction in the turbulent regime (Watanabe, Udagawa & Udagawa 1999; Balasubramanian, Miller & Rediniotis 2004; Gogte *et al.* 2005; Henoch *et al.* 2006; Daniello, Waterhouse & Rothstein 2009). Daniello *et al.* (2009) used a rectangular flow cell with smooth and superhydrophobic polydimethylsiloxane (PDMS) walls and studied flows from the laminar regime through transition and into the fully turbulent regime. They observed no drag reduction in the laminar regime because the channel height was much larger than the superhydrophobic feature size. However, in the turbulent regime, drag reductions of up to 50 % were observed with large slip velocities at the

superhydrophobic surface and slip lengths as large as $b = 100\,\mu$m. Drag reduction was found to increase with increasing Reynolds number before reaching an asymptote. These experimental and computational results suggest that in order for turbulent drag reduction to occur, the spacing between microfeatures must be on the same order as the thickness of the viscous sublayer (Daniello *et al.* 2009; Martell *et al.* 2010).

In addition to these turbulent channel flow experiments, there are three studies that investigated the flow past three-dimensional bodies coated with unstructured superhydrophobic surfaces at moderate to high Reynolds numbers. Gogte *et al.* (2005) observed drag reduction in turbulent flow over a hydrofoil coated with an superhydrophobic surface consisting of hydrophobically modified sandpaper. Drag reductions of up to 18 %, based on combined skin friction and form drag, were reported for the hydrofoil. The overall drag reduction on the hydrofoil decreased with increasing Reynolds number. However, only the total drag was reported and the individual contribution of friction and form drag were not deconvoluted. Similar results were observed by Balasubramanian *et al.* (2004) for flow over an ellipsoidal model coated with an unstructured superhydrophobic surface. In both studies, the superhydrophobic surfaces were unstructured, so the effect of systematic changes in feature size, spacing and solid fraction could not be studied. In addition, neither of these studies investigated the effect of slip on boundary-layer separation, which is the primary focus of this paper. More recently, McHale *et al.* (2009) used a similar surface to demonstrate up to 30 % drag reduction on a superhydrophobic sphere.

Two recent studies have numerically investigated the effect of slip on flow past circular cylinders. You & Moin (2007) used a combination of both DNS and large eddy simulations (LES) to investigate the flow past a circular cylinder containing alternating circumferential bands of partial slip and no-slip. The bands were placed with a period whose value was varied, but always on the order of a cylinder diameter. Additionally, the slip length was set to be 2 % of the cylinder diameter in both the streamwise and spanwise directions. At both the Reynolds numbers studied, slip was found to decrease the drag and r.m.s. lift on the cylinder by as much as 75 %. At the higher Reynolds numbers studied, the superhydrophobic surface was found to delay the separation point further downstream and reduce the base suction coefficient. Their study showed almost no effect on the shedding frequency or Strouhal number. Legendre, Lauga & Magnaudet (2009) used DNS to investigate circular cylinders with a partial slip boundary condition applied uniformly to the surface of the cylinder (no bands). Their simulations showed an increased drag reduction along with an increased vortex shedding frequency at a given Reynolds number with increasing slip length. Additionally, their simulations demonstrated that increasing slip length initially delayed the onset of the separated wake and vortex shedding to larger Reynolds numbers before eliminating the phenomena completely above a critical slip length.

Although no experimental investigations into the effects of slip on circular cylinders have been performed to date, there have been a number of attempts to reduce drag and vibrations on circular cylinders by modifying the surface roughness and texture. Many studies have focused on adding surface protrusions with different shapes and patterns (Zdravkovich 1981). Lim & Lee (2002) investigated the flow past circular cylinders with a series of U- and V-shaped grooves. Although the V-shaped groves had little effect, the U-shaped grooves proved to be quite effective. They produced a 20 % drag reduction at large Reynolds numbers ($Re > 5 \times 10^4$), a similar increase in the shedding frequency of the vortices and a significant elongation of the vortex

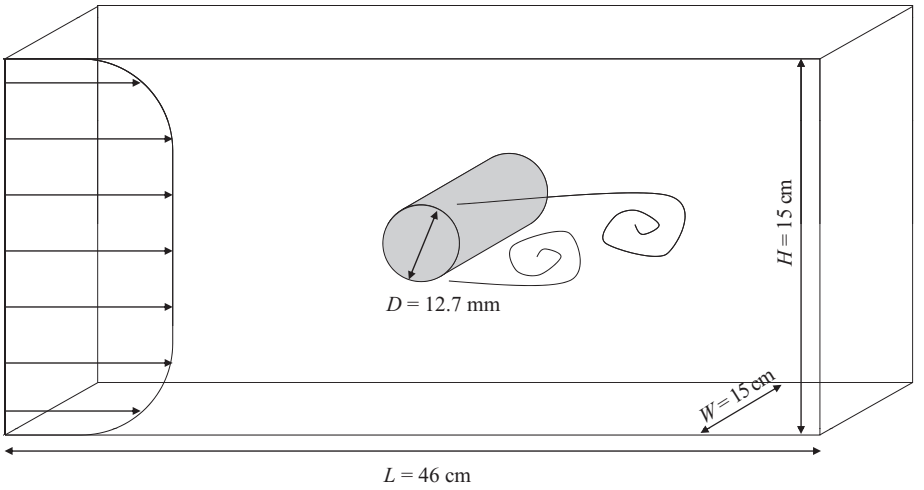

FIGURE 3. Schematic diagram of the flow cell. Both smooth cylinders and cylinders coated with superhydrophobic surfaces were tested.

formation region in the wake of the cylinder. These surfaces are similar in many respects to superhydrophobic surfaces, except that they are much larger in scale (mm versus μm) and fully wetted by the fluid. Thus, for these textured surfaces, unlike superhydrophobic surfaces, the effect of the flow is not the result of slip, but the result of the suppression of spanwise vortices in the wake of the cylinder (Lim & Lee 2002).

In this paper, we investigate the effect of slip on the separation and vortex dynamics downstream of a circular cylinder. Superhydrophobic surfaces of various sizes and spaced ridges aligned in both the flow direction and normal to the flow direction are tested. In § 2, the experimental set-up, design of the superhydrophobic surfaces and their fabrication is discussed. In § 3, the experimental results are presented and discussed in detail. Finally, in § 4 we conclude.

2. Experimental set-up

A water tunnel (Engineering Laboratory Design, Model 501) with a 15.2 cm × 15.2 cm × 45.7 cm test section was used for making both qualitative and quantitative measurements of flow past a circular cylinder with a velocity up to approximately $U = 1\ \mathrm{m\,s^{-1}}$, which corresponds to Reynolds numbers of approximately $Re = UD/\nu \leqslant 10\,000$. Here U is the average centreline velocity upstream of the cylinder measured with a Pitot tube, D is the diameter of the cylinder and ν is the viscosity of the water. A schematic diagram of the flow cell is shown in figure 3. The diameter of the circular cylinders was $D = 12.7$ mm, resulting in an aspect ratio of $W/D = H/D = 12$.

Soft lithography techniques were used to produce a series of precisely patterned superhydrophobic surfaces in PDMS (Xia & Whitesides 1998; Daniello *et al.* 2009). This lithographic technique is quite useful and flexible for producing patterns on the micron or even the nanometre length scales. The soft lithography process starts by using a CAD package to design the size, spacing and alignment of the desired micro-patterned surface. For these experiments, superhydrophobic surfaces were designed with two different sets of ridges. The first surface contained $d = 15\ \mu$m wide ridges spaced $w = 15\ \mu$m apart and the second contained $d = 30\ \mu$m wide ridges

spaced $w = 30\,\mu m$ apart. In addition to testing the effect of size and spacing of the superhydrophobic ridges, the effect of alignment of the ridges, both aligned and normal to the flow direction, was investigated. Once the design is completed, the CAD file is then printed on a high-resolution transparency at 5080 dpi. The transparency serves as a mask for contact photolithography using a positive photoresist (SU-8) on a silicon wafer (MacDonald & Muller 1997). The photoresist is exposed through the mask and developed, leaving behind a positive image of the mask in photoresist. At this point, the cross-linked photoresist remaining on the silicon can itself be used as the master to create a negative of its pattern in PDMS. This is done first by spin-coating the PDMS onto the silicon wafer and curing the PDMS in an oven. The replica is then peeled from the master, creating a micropatterned surface on a flexible elastomer substrate. It is naturally hydrophobic without further chemical reaction and it can be applied to almost any substrate or scaffold, flat or curved, while maintaining the ordered and precise patterning that makes the use of silicon wafers and lithographic techniques so desirable.

Because PDMS is a flexible rubber, it makes it possible to mold onto complex three-dimensional geometries. However, the single degree of curvature of the circular cylinder makes it ideal for coating because it eliminates the need for complicated cutting, folding and seaming of the superhydrophobic surfaces. A single seam does exist running axially along the length of the cylinder. Special care was taken to minimize the height of the seam which was kept below approximately $50\,\mu m$ along its entire length. The seam was placed at the rear stagnation point of the cylinder, $\theta = 180^\circ$. The impact of the seam was studied by comparing the separation and shedding frequency for both a smooth aluminium cylinder and smooth PDMS-coated cylinder containing a seam. No discernible difference between these two cylinders could be measured, suggesting that the presence of the small seam does not have a large impact on the flow when placed along the trailing edge of the cylinder.

There are a number of experimental challenges associated with maintaining a coherent air–water interface. The microfeatures on a superhydrophobic surface are susceptible to damage occurring during installation or operation as well as defects introduced during fabrication. Posts are especially vulnerable which is why we have focused on ridges in this study. If a superhydrophobic surface is operating near the maximum static pressure for which an air–water interface can be maintained and a single post is missing or damaged, the spacing between posts will double locally and the entire superhydrophobic surface can be wetted by water, thereby destroying its efficacy. In order to mitigate this problem, we have instituted a novel improvement to superhydrophobic surface design which makes the surface more robust, less prone to catastrophic damage and capable of supporting significantly larger static or dynamic pressures, therefore increasing the range of applications and uses for superhydrophobic drag reduction.

Our design is quite simple incorporating what we call breaker ridges shown schematically in figure 4. There is a large difference in drag reduction if a ridge is aligned in the flow direction or normal to the flow direction. In laminar flow, if the ridges are aligned with the flow, they are twice as effective as ridges aligned against the flow direction (Lauga & Stone 2003). In turbulent flow, ridges aligned normal to the flow direction actually increase drag (Min & Kim 2004) while ridges aligned in the flow direction can greatly reduce drag up to 50 % as we have shown (Daniello *et al.* 2009). In the case of a superhydrophobic surface containing ridges, our surface design incorporates both ridges in the flow direction and normal to it, as seen schematically in figure 4. We call the ridges across the flow direction, breaker ridges. For the case

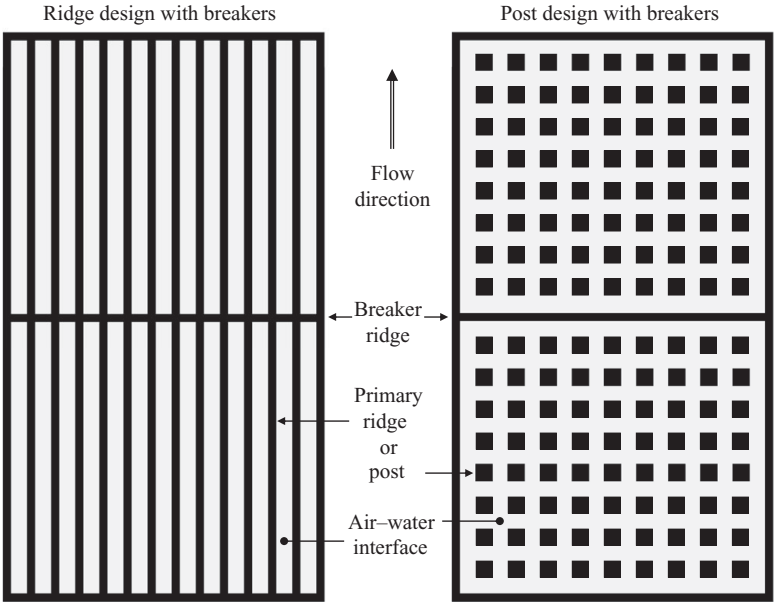

FIGURE 4. A schematic diagram of superhydrophobic designs with breaker ridges used for arrays of ridges in the flow direction or posts.

of arrays of posts, the breaker ridges form a bounding box. The breaker ridges were added at intervals of 2 mm, which is roughly two orders of magnitude larger than the spacing between the primary ridges. The relatively low density of breaker ridges means that they should have very little impact on the drag reduction of the surface, but have a significant impact on the ability of the surface to maintain the air–water interface, which is critical for the purpose of these surfaces.

The novelty of this design is that the breaker ridges will isolate any failure of interface between the primary ridges to the region between two breaker ridges. Thus, for a surface as in figure 4 with ridges spaced 15 μm apart failures can be isolated to regions as small as 2 mm. Breaker ridges trap the air within a closed cavity. Because the air has nowhere to go, any deformation of the air–water interface will compress the trapped air and raise the pressure within the cavity. The increase in air pressure, which we can assume is an ideal gas, increases inversely with the changing volume of the cavity, $P_{air} \propto 1/V_{air}$. Thus, a 10 % reduction in the cavity size will increase the cavity pressure by 10 %. For a very deep cavity this does not have much of an effect, but for our ridges which are half as deep as they are spaced apart, this can have a significant effect. Additionally, this means that even under high pressure, the air can be compressed, but is not lost. Without the breakers it would be driven out at the open ends of the ridge, however far apart they may be. An additional benefit of these breaker ridges is that they make the surfaces more robust. We are currently fabricating our surfaces out of PDMS, which has a relatively large elastic modulus; however, in a turbulent flow the shear stress and pressure fluctuations can deform the ridges or posts especially in high-Reynolds-number flows or when the ridges are reduced in size. By adding the breaker ridges, the primary ridges are converted from individual ridges to a box section which is significantly stronger and less likely to deform or buckle.

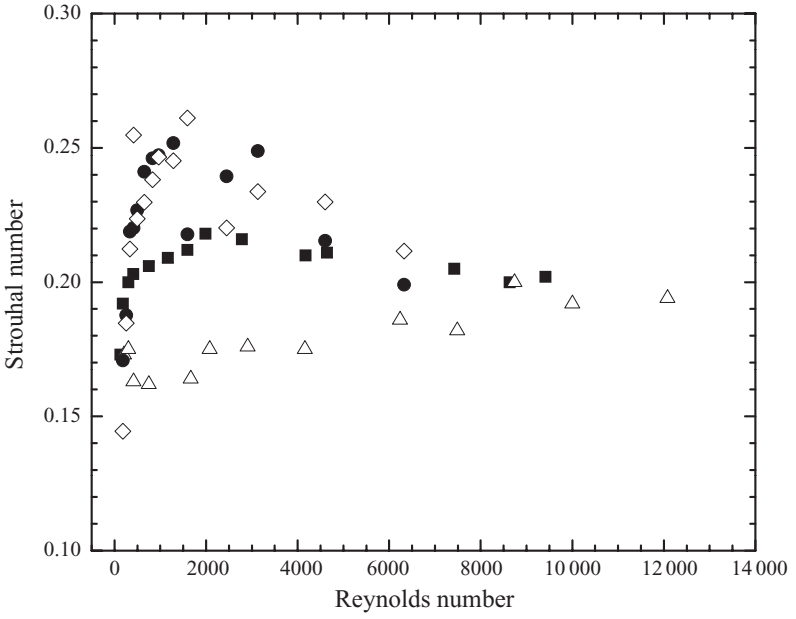

FIGURE 5. Dimensionless vortex shedding frequency, Strouhal number, as a function of Reynolds number for a circular cylinder with a smooth surface (■) and superhydrophobic surfaces containing $w = 30\,\mu m$ wide microridge spaced $d = 30\,\mu m$ apart (◇) and $w = 15\,\mu m$ wide microridge spaced $d = 15\,\mu m$ apart aligned in the flow direction (●) as well as $w = 15\,\mu m$ wide microridge spaced $d = 15\,\mu m$ apart aligned normal to the flow direction (△).

3. Results and discussion

As described by the excellent review of Williamson (1996), amongst others, a number of different flow regimes exist for the flow past a no-slip circular cylinder. The transition to each flow regime has been quantified and the vortex dynamics studied in great detail. Below a Reynolds number of approximately $Re < 5$, the flow does not separate. Between $5 < Re < 49$, the wake behind the cylinder contains two steady, counter-rotating vortices. Beyond a Reynolds number of $Re > 49$, the steady vortices in the wake of the cylinder become unstable and a laminar vortex shedding regime persists up to a Reynolds number of about $Re \approx 200$. In this regime, A-mode vortices are shed at a dimensionless shedding frequency known as the Strouhal number, $St = f\,D/U$, which increases with increasing Reynolds numbers. This can be seen in the measurements for Strouhal number for a smooth surface presented in figure 5, which match the well-established trends in the literature (Williamson 1996). The A-mode is characterized by spanwise wavelength of the secondary vortices that can be several cylinder diameters. At larger Reynolds numbers, B-mode vortices become the dominant mode and are characterized by spanwise wavelengths approximately one cylinder in diameter (Brede, Eckelmann & Rockwell 1996). As the Reynolds number continues to increase, the flow in the wake of the cylinder becomes increasingly three-dimensional and disordered. Above a Reynolds number of approximately $Re > 1000$, the shear layer passing around the cylinder becomes unstable, the wake becomes fully turbulent, the separation point moves upstream along the cylinder and the Strouhal number begins to decrease slowly with increasing Reynolds number (Williamson 1996). Tracking the changes to the Strouhal number scaling with Reynolds number

Surface	Smooth	15–15 μm Ridges aligned in flow direction	30–30 μm Ridges aligned in flow direction	15–15 μm Aligned normal to flow direction
Critical Reynolds number for onset of vortex shedding	<70	70–90	70–90	<70

TABLE 1. Critical Reynolds number for the onset of vortex shedding for the flow past both a smooth circular cylinder and circular cylinders coated with a series of different superhydrophobic surfaces. The minimum attainable flow speed resulted in a Reynolds number of $Re_{min} = 70$ and the speed could be increased by increments of $Re = 20$, resulting in the range of critical Reynolds number values presented in the table.

is an excellent starting point for quantifying the effect of slip on the cylinder surface (Legendre, Lauga & Magnaudet 2009).

In order to quantify the onset and frequency of shedding of the primary vortices, the fluid was seeded with 50 μm diameter neutrally buoyant silvered glass spheres (Sphericel, Potters Industries, Carlstadt, NJ). The particles were illuminated using a 500 μm laser light sheet and their motion captured using a high-speed video camera (Phantom V4.2). A commercial particle image velocimetry (PIV) code (DaVis, LaVision Gmbh) was then used to correlate the particle displacements and calculate both velocity vector fields and vorticity fields. Proper orthogonal decomposition (POD) was then used to isolate the primary vortices and determine their shedding frequency and the Strouhal number (Shi, Liu & Wan 2010). Streak images were also captured using a digital camera (Nikon D70) set to long exposure times. Although the water tunnel, running at its lowest setting, was not capable of capturing the onset of flow separation, the streak images could be used to determine the critical Reynolds number for the onset of vortex shedding for both the smooth and superhydrophobic surfaces used.

The critical Reynolds numbers for the onset of vortex shedding are presented in table 1 within the velocity and Reynolds number resolution of the water tunnel. The lower limit in velocity of the water tunnel corresponded to a Reynolds number of $Re_{min} = 70$ and the minimum possible velocity increment corresponded to an increase of 20 in Reynolds number. The precision to which we can determine the critical Reynolds number for the onset of vortex shedding is less than optimal. However, these measurements clearly demonstrate that by coating a cylinder with a superhydrophobic surface and inducing slip along the surface of the circular cylinder, the onset of vortex shedding is delayed to larger Reynolds numbers. The largest shift is observed for the 30–30 μm superhydrophobic surface for which the critical Reynolds number has been observed to shift from around $Re = 70$ for the smooth surface to between 70 and 90. Of the surfaces tested, this surface has been shown to produce the largest slip lengths and drag reductions in both laminar and turbulent channel flows (Ou & Rothstein 2005; Daniello *et al.* 2009). No observable shift in the critical Reynolds number was observed for the surface containing ridges aligned perpendicular to the flow direction. This result agrees qualitatively with the literature where increasing the amount of slip along the cylinder has been shown in DNS to delay the onset of both flow separation and vortex shedding (Legendre *et al.* 2009). Unfortunately, because of the uncertainty in the exact value of the critical Reynolds number in the experiments, a direct comparison with the literature is not possible at this point.

The formation of the separated wake and the onset of vortex shedding are a consequence of vorticity accumulation downstream of the cylinder (Leal 1989). In fact, it has been shown for a number of bluff bodies that separation and the onset of shedding occur when the vorticity generated from the surface of the bluff body exceeds a value that is of the order of $\omega_{s,max} \approx 5\,U/R$ (Leal 1989; Magnaudet & Mougin 2007; Legendre *et al.* 2009). For a no-slip surface at large Reynolds numbers, the amount of vorticity generated at the surface is proportional to the shear stress along the surface and is known to increase like $\omega_s \approx (U/R)\ Re^{1/2}$ with Reynolds number (Leal 1992). For a shear-free surface, vorticity is still generated, not by skin friction which is set to be zero, but by the need to rotate fluid elements along curved streamlines. Specifically, by forcing the tangential shear stress to vanish along the wall of a curved body, a direct relationship between the velocity gradient and the slip velocity results, which is dependent on the surface curvature. For a cylinder or a sphere with a perfect slip boundary condition, the vorticity generated on the surface becomes $\omega_s = 2\,(U_s/R)$, where U_s is the slip velocity along the cylinder. Interestingly, for a perfect slip cylinder, the magnitude of the dimensionless vorticity, $\omega_s/(U_s/R)$, does not increase with increasing Reynolds number and it remains below the critical vorticity needed to produce either a steady or an unsteady separated wake (Legendre *et al.* 2009). This has also been observed numerically in flows past shear-free undeformable spheres. However, in experimental measurements of droplet dynamics the free surface can deform significantly. This can in turn reduce the radius of curvature near the trailing edge of the droplet or bubble and increase the vorticity generated enough to result in separation and vortex shedding (Leal 1989; Magnaudet & Mougin 2007). In our experiments, we do not have a perfect slip boundary condition, but a partial slip condition with a slip length that has been measured in flows past flat plates to be around $b = 100\,\mu\text{m}$. Thus, some hybrid behaviour between the limits of no-slip and shear-free is expected and is indeed observed. This can be seen most clearly in the vortex dynamics after the onset of shedding.

As shown in figure 5, for the smooth circular cylinder, the Strouhal number follows the expected trends; first increasing rapidly at low Reynolds numbers before reaching a maximum and slowly decreasing with continued increase in Reynolds number. The application of superhydrophobic coatings to the surface of the circular cylinder has a significant effect on the vortex shedding dynamics. This can be seen quite clearly from the Strouhal number in figure 5. Using superhydrophobic surfaces with ridges aligned in the flow direction increases the Strouhal number by as much as 25 % from $St = 0.2$ to $St = 0.25$ at a Reynolds number of $Re = 1000$. The increase in the Strouhal number is observed starting at a Reynolds number of $Re = 300$ and is maintained for all the Reynolds numbers tested, although the magnitude of the increase in the Strouhal number is found to decrease as the Reynolds number increases beyond $Re > 2000$. The reversal of this trend below $Re < 300$ is probably the result of delay in the onset of vortex shedding for this superhydrophobic surface. The overall effect on Strouhal number seems to be nearly independent of the size and spacing of the microridges, with both the 15–15 μm and 30–30 μm ridges showing similar enhancement to the Strouhal number. However, it is clear from figure 5 that the alignment of the microstructure on the superhydrophobic surface plays a significant role in the vortex dynamics. In laminar flows, aligning the ridges normal to the flow direction reduces the drag reduction by a factor of two (Lauga & Stone 2003), while in turbulent flows, DNS simulations have shown that transverse ridges significantly reduce the slip velocity on the superhydrophobic surface while essentially eliminating the drag reduction (Martell *et al.* 2010) or in some instances increasing

the drag (Min & Kim 2004). Additionally, the alignment of the ridges normal to the flow direction enhances the axial velocity fluctuations along the ridges. As seen in figure 5, for the superhydrophobic ridges aligned axially along the cylinder and normal to the flow direction, the trend in the Strouhal number is quite different. In this case a 25 % reduction in the Strouhal number is observed at a Reynolds number of $Re = 1000$ with the effect of the superhydrophobic surface again slowly diminishing as the Reynolds number is increased to $Re = 10\,000$.

Thus, although we anticipate that the superhydrophobic coating will reduce the drag and the r.m.s. lift on the cylinders, the presence of ridges aligned in the flow direction was found to increase the frequency of vortex shedding from the cylinder. The increase in the Strouhal number is directly related to slip velocity induced along the surface of the superhydrophobic cylinders. The Strouhal number is proportional to the time rate of change of vorticity at the cylinder surface which is in turn a function of both the diffusion of vorticity across the boundary layer and the advection of vorticity along the cylinder. The diffusion is almost unaffected by slip, although mixing and enhanced vorticity diffusion can be induced by the flow across transverse ridges (Ou, Moss & Rothstein 2007), perhaps accounting for some of the differences observed here between ridges aligned with and against the flow direction. The advection of vorticity along the cylinder, on the other hand, increases linearly with increasing slip velocity. Legendre *et al.* (2009) derived an approximate expression for the slip velocity on a cylinder as a function of slip length and Reynolds number. They showed that $U_s/U \propto \alpha Re^{1/2}/(\alpha Re^{1/2} + 1 + R/b)$, where α is an order-one constant. Thus, a larger effect on the Strouhal number is expected for increasing positive or negative slip lengths and decreasing Reynolds numbers. This analysis helps explain why the effect of slip diminishes as the Reynolds number and the boundary-layer thickness increase.

The effect of the superhydrophobic surface on the vortex shedding dynamics can be further investigated by comparing streak images from the different cylinders at a fixed Reynolds number. In figures 6 and 7, streak images for Reynolds numbers of $Re = 180$ and $Re = 490$ are presented for comparison. The differences in these images are quite striking. First, note that the formation region of the separated vortex is much larger for the superhydrophobic surfaces. The end of the formation region is defined as the location along the centreline where oscillating wake characteristics are first observed (Lim & Lee 2002). Increases in the size of the formation region have been shown to directly correlate to a reduction in drag (Lim & Lee 2002). One consequence of the increased length of the formation region is that the vortices shed from the superhydrophobic cylinders are significantly elongated/stretched in the flow direction, both before and after the onset of vortex shedding. This is probably caused by the slip velocity along the cylinder and the resulting increased velocity within the boundary layer. A final observation is that the degree of interlacing of the shed vortices downstream of the superhydrophobic cylinders is significantly reduced. In other words, the centres of the vortices shed from the superhydrophobic cylinders are offset further from the centreline than vortices from the smooth cylinder. These observations, which are perhaps more easily observed in the PIV velocity vector fields presented in figure 8, might also suggest a reduction in the strength of the r.m.s. lift force. Future experiments are planned to directly measure both the drag and lift forces on all the cylinders tested in this study.

From the streak images in figures 6 and 7, it is also possible to observe changes in the separation point from the cylinder as a function of superhydrophobic coating. The separation point is quantified in figure 9 as a function of the Reynolds number for

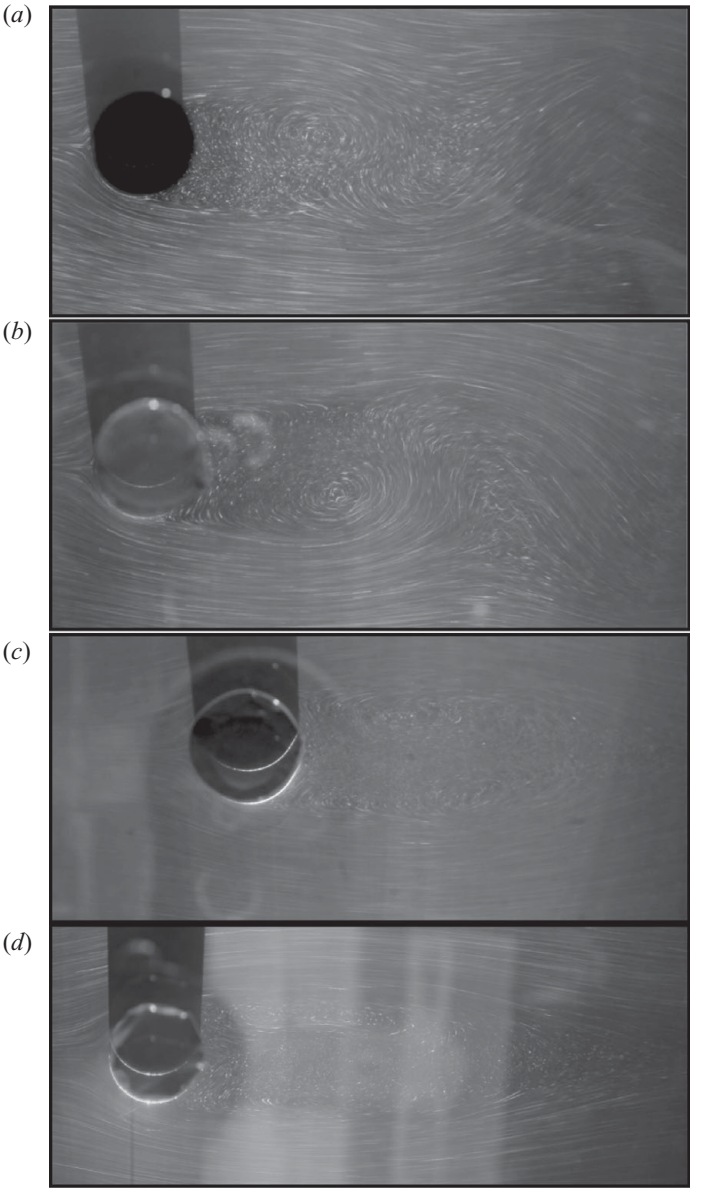

FIGURE 6. Streak images showing flow separation and vortex shedding past a series of cylinders at a Reynolds number of $Re = 180$. The images include (*a*) a smooth cylinder, (*b*) a superhydrophobic cylinder containing 15 μm wide ridges spaced 15 μm apart and aligned in the flow direction, (*c*) a superhydrophobic cylinder containing 30 μm wide ridges spaced 30 μm apart and aligned in the flow direction, and (*d*) a superhydrophobic cylinder containing 15 μm wide ridges spaced 15 μm apart and aligned perpendicular to the flow direction.

the smooth cylinder as well as the three superhydrophobic cylinders. The separation point from the smooth cylinder follows the well-established trends. Near the onset of vortex shedding, the separation angle is approximately $\theta_{sep} = 110^\circ$. Here $\theta_{sep} = 0^\circ$ corresponds to the stagnation point at the leading edge of the cylinder. It should also be noted that all the separation angle measurements were only accurate within $\pm 1^\circ$.

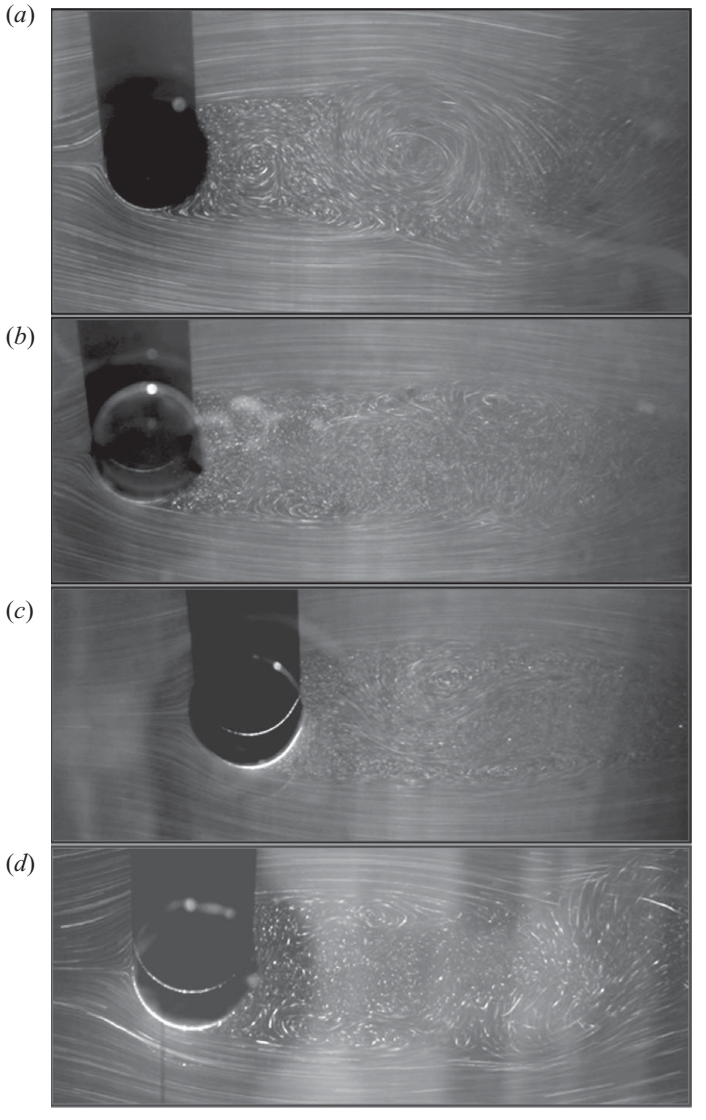

FIGURE 7. Streak images showing flow separation and vortex shedding past a series of cylinders at a Reynolds number of $Re = 493$. The images include (*a*) a smooth cylinder, (*b*) a superhydrophobic cylinder containing 15 μm wide ridges spaced 15 μm apart and aligned in the flow direction, (*c*) a superhydrophobic cylinder containing 30 μm wide ridges spaced 30 μm apart and aligned in the flow direction, and (*d*) a superhydrophobic cylinder containing 15 μm wide ridges spaced 15 μm apart and aligned perpendicular to the flow direction.

With increasing Reynolds number, the separation point moves very quickly upstream, past the equator and eventually asymptotes around $\theta_{sep} = 85°$. The separation point measured for the superhydrophobic surfaces follow the same general trend; however, for the surfaces with ridges aligned in the flow direction, the separation angle is consistently smaller at all but the smallest Reynolds numbers. This is probably the result of the slip velocity at the surface of the cylinder, increasing the velocity and linear momentum of the fluid within the boundary layer or perhaps reducing the

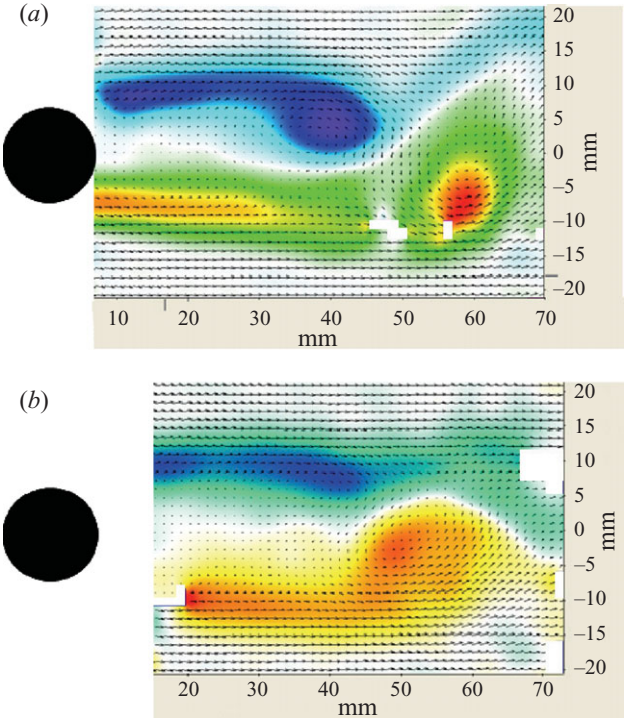

FIGURE 8. (Colour online available at journals.cambridge.org/FLM) For caption see next page.

base suction. Just the opposite trend is observed for the superhydrophobic surface containing ridges aligned normal to the flow direction; the separation angle retreats more slowly and asymptotes at a slightly larger value than for both the smooth and other superhydrophobic surfaces. Another interesting observation is that the 15 μm ridges appear to have a more significant impact on the separation angle than the 30 μm ridges. At least at the lower Reynolds numbers, this is probably the result of the significant delay observed in the onset of vortex shedding. However, at high Reynolds numbers, it may be a result of the gradual failure of this surface on the front stagnation point at high Reynolds numbers where the stagnation pressure was enough to drive the air–water interface into the spaces between some of the ridges and transition the superhydrophobic surface from a Cassie to a Wenzel state. With the cylinder underwater, the air–water interface between ridges is highly reflective and appears to shimmer. The transition from Cassie to Wenzel state coincides with a change in the appearance of the surface from reflective to matte black which is the colour of the PDMS. For the superhydrophobic surface with 30 μm ridges, above a Reynolds number of $Re = 4000$ roughly 10 % of the surface around the leading edge of the cylinder was gradually driven into the Wenzel state. The 15 μm ridges were found to remain in the Cassie state over all the Reynolds numbers tested.

4. Conclusions

In this work, we performed a series of experiments to investigate the influence of slip on the flow past a circular cylinder. The partial slip boundary condition was produced

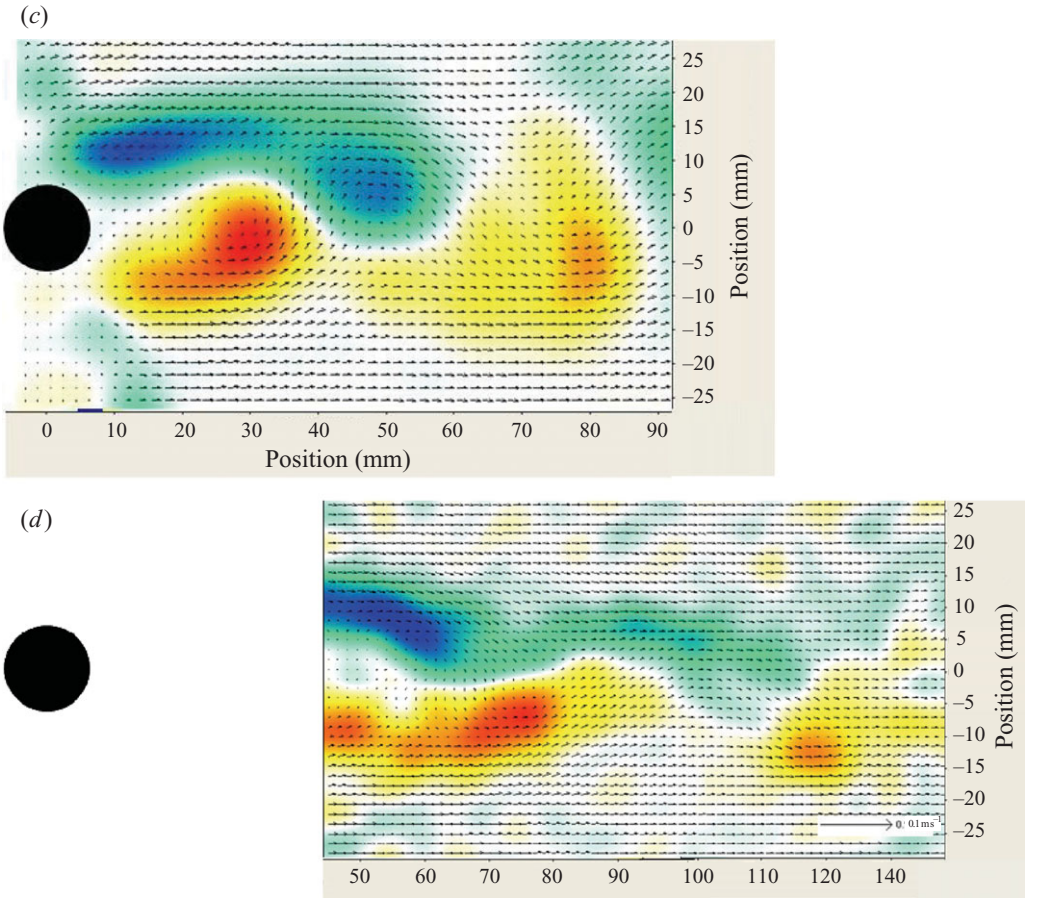

FIGURE 8. (Colour online) PIV vector fields with vorticity overlaid as a colour map. The vector fields were correlated downstream of (*a*) a smooth circular cylinder, (*b*) a superhydrophobic cylinder containing 15 µm wide ridges spaced 15 µm apart and aligned perpendicular to the flow direction, (*c*) a superhydrophobic cylinder containing 15 µm wide ridges spaced 15 µm apart and aligned in the flow direction, and (*d*) a superhydrophobic cylinder containing 30 µm wide ridges spaced 30 µm apart and aligned in the flow direction at a Reynolds number of $Re = 256$.

by coating the circular cylinder with a series of superhydrophobic surfaces patterned with ridges aligned both tangent and normal to the flow direction. When compared with smooth cylinders, these experiments demonstrated that slip delays the onset of vortex shedding in the wake of the cylinder to higher Reynolds numbers and increases the length of the recirculation region in the wake of the cylinder. In addition, for surfaces with ridges aligned in the flow direction, the shedding frequency was found to increase while the separation point moved further upstream. The opposite trends were observed for the cylinder with ridges aligned normal to the flow direction. This work demonstrated experimentally that slip at the surface of the circular cylinder can have a strong impact on the vortex shedding dynamics. Future work is planned to measure the impact these surfaces have on both the drag and the r.m.s. lift produced by the shedding vortices.

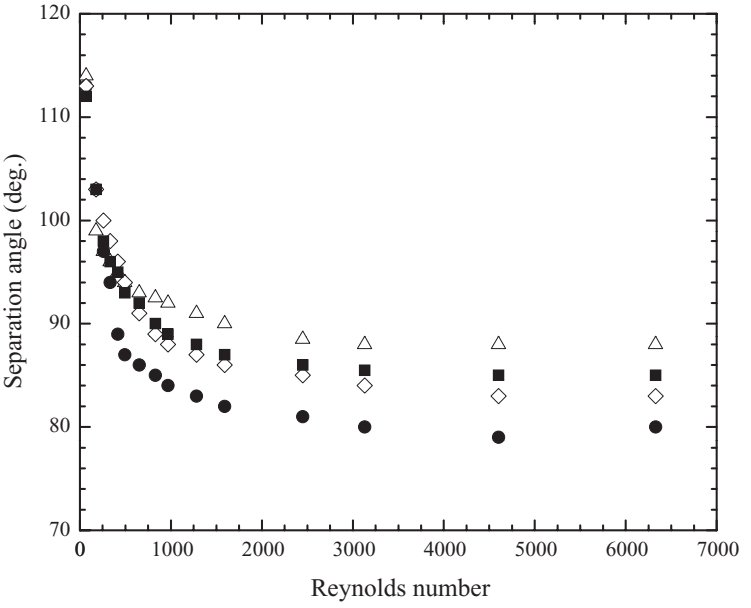

FIGURE 9. Separation angle as a function of the Reynolds number for a circular cylinder with a smooth surface (■) and superhydrophobic surfaces containing $w = 30\,\mu$m wide microridge spaced $d = 30\,\mu$m apart (◇) and $w = 15\,\mu$m wide microridge spaced $d = 15\,\mu$m apart aligned in the flow direction (●) as well as $w = 15\,\mu$m wide microridge spaced $d = 15\,\mu$m apart aligned normal to the flow direction (△). Separation angle is measured from the upstream stagnation point of the cylinder.

The authors wish to acknowledge the National Science Foundation and the Office of Naval Research for the partial support of this research under grants CBET-0967531 and N00014-06-1-0497, respectively.

REFERENCES

BALASUBRAMANIAN, A. K., MILLER, A. C. & REDINIOTIS, O. K. 2004 Microstructured hydrophobic skin for hydrodynamic drag reduction. *AIAA J.* **42**, 411–414.

BARTHLOTT, W. & NEINHUIS, C. 1997 Purity of the sacred lotus, or escape from contamination in biological surfaces. *Planta* **202**, 1–8.

BÉNARD, H. 1908 The formation of gyration centres at the back of a moving obstacle. *C. R. Acad. Sci.* **147**, 839–842.

BHUSHAN, B. & JUNG, Y. C. 2006 Micro- and nanoscale characterization of hydrophobic and hydrophilic leaf surfaces. *Nanotech.* **17**, 2758–2772.

BICO, J., MARZOLIN, C. & QUERE, D. 1999 Pearl drops. *Europhys. Lett.* **47**, 220–226.

BREDE, M., ECKELMANN, H. & ROCKWELL, D. 1996 On secondary vortices in the cylinder wake. *Phys. Fluids* **8**, 2117–2124.

CASSIE, A. B. D. & BAXTER, S. 1944 Wettability of porous surfaces. *Trans. Faraday Soc.* **40**, 546–551.

CHOI, C. H. & KIM, C. J. 2006 Large slip of aqueous liquid flow over a nanoengineered superhydrophobic surface. *Phys. Rev. Lett.* **96**, 066001.

CHOI, C.-H., ULMANELLA, U., KIM, J., HO, C.-M. & KIM, C.-J. 2006 Effective slip and friction reduction in nanograted superhydrophobic microchannels. *Phys. Fluids* **18**, 087105.

DANIELLO, R., WATERHOUSE, N. E. & ROTHSTEIN, J. P. 2009 Turbulent drag reduction using superhydrophobic surfaces. *Phys. Fluids* **21**, 085103.

FUKAGATA, K., KASAGI, N. & KOUMOUTSAKOS, P. 2006 A theoretical prediction of friction drag reduction in turbulent flow by superhydrophobic surfaces. *Phys. Fluids* **18**, 051703.

Gogte, S., Vorobieff, P., Truesdell, R., Mammoli, A., van Swol, F., Shah, P. & Brinker, C. J. 2005 Effective slip on textured superhydrophobic surfaces. *Phys. Fluids* **17**, 051701.

Henoch, C., Krupenkin, T. N., Kolodner, P., Taylor, J. A., Hodes, M. S., Lyons, A. M., Peguero, C. & Breuer, K. S. 2006 Turbulent drag reduction using superhydrophobic surfaces. In *AIAA Flow Control Conference*, San Francisco, CA.

Joseph, P., Cottin-Bizonne, C., Benoit, J.-M., Ybert, C., Journet, C., Tabeling, P. & Bocquet, L. 2006 Slippage of water past superhydrophobic carbon nanotube forests in microchannels. *Phys. Rev. Lett.* **97**, 156104.

von Kármán, T. 1911 Uber den mechanismus den widerstands, den ein bewegter korper in einer flussigkeit erfahrt. *Gottingen Nachr. Math. Phys. Kl.* **12**, 509–517.

Lauga, E. & Stone, H. A. 2003 Effective slip in pressure driven stokes flow. *J. Fluid Mech.* **489**, 55–77.

Leal, L. G. 1989 Vorticity transport and wake structure for bluff bodies at finite Reynolds number. *Phys. Fluids* **1**, 124–131.

Leal, L. G. 1992 *Laminar Flow and Convective Transport Processes: Scaling Principles and Asymptotic Analysis.* Butterworth-Heinemann.

Lee, C. & Kim, C.-J. 2009 Maximizing the giant liquid slip on superhydrophobic microstructures by nanostructuring their sidewalls. *Langmuir* **25**, 12 812–12 818.

Legendre, D., Lauga, E. & Magnaudet, J. 2009 Influence of slip on the dynamics of two-dimensional wakes. *J. Fluid Mech.* **633**, 437–447.

Lim, H.-C. & Lee, S. J. 2002 Flow control of circular cylinders with longitudinal grooved surfaces. *AIAA J.* **40**, 2027–2036.

MacDonald, M. J. & Muller, S. J. 1997 Shear rheology of polymer solutions near the critical condition for elastic instability. *Rheol. Acta* **36**, 97–109.

Magnaudet, J. & Mougin, G. 2007 Wake instability of a fixed spheroidal bubble. *J. Fluid Mech.* **572**, 311–337.

Martell, M. B., Perot, J. B. & Rothstein, J. P. 2009 Direct numerical simulations of turbulent flows over superhydrophobic surfaces. *J. Fluid Mech.* **620**, 31–41.

Martell, M. B., Rothstein, J. P. & Perot, J. B. 2010 An analysis of superhydrophobic turbulent drag reduction mechanisms using direct numerical simulation. *Phys. Fluids* **22**, 065102.

McHale, G., Shirtcliffe, N. J., Evans, C. R. & Newton, M. I. 2009 Terminal velocity and drag reduction measurements on superhydrophobic spheres. *App. Phys. Lett.* **94**, 064104.

Min, T. & Kim, J. 2004 Effects of hydrophobic surfaces on skin-friction drag. *Phys. Fluids* **16**, L55–L58.

Navier, C. L. M. H. 1823 Memoire sur les lois du mouvement des fluides. *Mem. Acad. R. Sci. Inst. Fr.* **6**, 389–440.

Oner, D. & McCarthy, T. J. 2000 Ultrahydrophobic surfaces: effects of topography length scales on wettability. *Langmuir* **16**, 7777–7782.

Ou, J., Moss, G. R. & Rothstein, J. P. 2007 Enhanced mixing in laminar flows using ultrahydrophobic surfaces. *Phys. Rev.* E **76**, 016304.

Ou, J., Perot, J. B. & Rothstein, J. P. 2004 Laminar drag reduction in microchannels using ultrahydrophobic surfaces. *Phys. Fluids* **16**, 4635–4660.

Ou, J. & Rothstein, J. P. 2005 Direct velocity measurements of the flow past drag-reducing ultrahydrophobic surfaces. *Phys. Fluids* **17**, 103606.

Pope, S. B. 2003 *Turbulent Flows.* Cambridge University Press.

Rothstein, J. P. 2010 Slip on superhydrophobic surfaces. *Annu. Rev. Fluid Mech.* **42**, 89–109.

Shi, L. L., Liu, Y. Z. & Wan, J. J. 2010 Influence of wall proximity on characteristics of wake behind a square cylinder: PIV measurements and POD analysis. *Exp. Therm. Fluid Sci.* **34**, 28–36.

Strouhal, V. 1878 Uber eine besondere art der tonerregung. *Annal. Physik Chemie* **5**, 216–251.

Truesdell, R., Mammoli, A., Vorobieff, P., van Swol, P. & Brinker, C. J. 2006 Drag reduction on a patterned superhydrophobic surface. *Phys. Rev. Lett.* **97**, 044504.

Watanabe, K., Udagawa, Y. & Udagawa, H. 1999 Drag reduction of Newtonian fluid in a circular pipe with highly water-repellent wall. *J. Fluid Mech.* **381**, 225–238.

Wenzel, R. N. 1936 Resistance of solid surfaces to wetting by water. *Ind. Engng Chem.* **28**, 988–994.

Williamson, C. H. K. 1996 Vortex dynamics in the cylinder wake. *Annu. Rev. Fluid Mech.* **28**, 477–539.

Xia, Y. & Whitesides, G. 1998 Soft lithography. *Annu. Rev. Mater. Sci.* **28**, 153–84.

Ybert, C., Barentin, C., Cottin-Bizonne, C., Joseph, P. & Bocquet, L. 2007 Achieving large slip with superhydrophobic surfaces: scaling laws for generic geometries. *Phys. Fluids* **19**, 123601.

You, D. & Moin, P. 2007 Effects of hydrophobic surfaces on the drag and lift of a circular cylinder. *Phys. Fluids* **19**, 081701.

Zdravkovich, M. M. 1981 Review and classification of various aerodynamics and hydrodynamic means for suppressing vortex shedding. *J. Wind Engng Ind. Aerodyn.* **7**, 145–189.

Zhang, X., Shi, F., Niu, J., Jiang, Y. & Wang, Z. 2008 Superhydrophobic surfaces: from structural control to functional application. *J. Mater. Chem.* **18**, 621–633.